Available online at www.sciencedirect.com

SciVerse ScienceDirect

Journal of the European Ceramic Society 32 (2012) 1701–1709

www.elsevier.com/locate/jeurceramsoc

Lanthanum nickelate thin films deposited by spray pyrolysis: Crystallization, microstructure and electrochemical properties

Thomas Ryll [a,*], Philipp Reibisch [a], Lukas Schlagenhauf [a], Anja Bieberle-Huetter [a], Max Döbeli [b], Jennifer L.M. Rupp [a], Ludwig J. Gauckler [a]

[a] *Nonmetallic Inorganic Materials, Department of Materials, ETH Zurich, Wolfgang-Pauli-Strasse 10, 8093 Zurich, Switzerland*
[b] *Laboratory of Ion Beam Physics, Department of Physics, ETH Zurich, Schafmattstrasse 20, 8093 Zurich, Switzerland*

Received 31 August 2011; received in revised form 13 December 2011; accepted 29 December 2011
Available online 23 January 2012

Abstract

Thin films from the $La_{n+1}Ni_nO_{3n+1}$ system exhibit favorable dielectric and electrochemical properties that may prove useful for a variety of devices ranging from ferroelectrics to low-temperature solid oxide fuel cells. The present work covers the compositional, microstructural and electrochemical characterization of thin lanthanum nickelate films deposited by spray pyrolysis. In accordance with the phase diagram, $LaNiO_{3-\delta}$ or $La_4Ni_3O_{10-\delta}$ films were obtained during annealing of spray deposited films at temperatures between 540 °C and 1100 °C. Whereas $LaNiO_{3-\delta}$ films exhibited a high metallic conductivity, $La_4Ni_3O_{10-\delta}$ films were semiconducting. Electrochemical impedance spectroscopy indicated an increase of the area specific oxygen reduction resistance with the annealing temperature. The study highlights how the phase and microstructure of thin films from the $La_{n+1}Ni_nO_{3n+1}$ system can be tailored by annealing of initially amorphous films. $LaNiO_{3-\delta}$ films have a high potential for application in electrochemical devices operating at low temperatures where high electrical conductivity is required.

Keywords: Thin films; Sol–gel processes; Electrical conductivity; Fuel cells; Transition metal oxides

1. Introduction

Due to promising electrical and catalytic properties materials from the lanthanum nickelate system $La_{n+1}Ni_nO_{3n+1}$ ($1 \leq n < \infty$) have attracted considerable attention within the past decades. Whereas thin films of the perovskite phase $LaNiO_{3-\delta}$ ($n \rightarrow \infty$) have been applied as electrodes for ferroelectric devices, thin-film capacitors and superconducting films,[1–3] the higher order Ruddlesden–Popper phases $La_4Ni_3O_{10-\delta}$ ($n=3$) and $La_3Ni_2O_{7-\delta}$ ($n=2$) show great promise for application as cathodes in intermediate temperature solid-oxide fuel cells (SOFCs).[4,5]

$LaNiO_{3-\delta}$ adopts a rhombohedral perovskite structure and exhibits a metallic conductivity of 600 S cm^{-1} at room temperature.[6–9] During heating, $LaNiO_{3-\delta}$ decomposes forming the Ruddlesden–Popper phases with $n=3$, 2 and 1, corresponding to the consecutive reactions (1) → (2) → (3).[10] The equilibrium temperatures for the reactions (1)–(3) in air are 978, 1183 and 1231 °C, respectively.[11]

$$4LaNiO_{3-\delta} \rightarrow La_4Ni_3O_{10-\delta} + NiO + 0.5O_2 \quad (1)$$

$$3La_4Ni_3O_{10-\delta} \rightarrow 4La_3Ni_2O_{7-\delta} + NiO + 0.5O_2 \quad (2)$$

$$2La_3Ni_2O_{7-\delta} \rightarrow 3La_2NiO_{4+\delta} + NiO + 0.5O_2 \quad (3)$$

The Ruddlesden–Popper structure is composed of n layers of the perovskite $LaNiO_{3-\delta}$ permeated by single LaO layers with rocksalt structure.[7,12] With decreasing n, the electrical conductivity decreases and a successive change from metallic to semiconducting behavior occurs.[4–6] In contrast to the pure perovskite, the Ruddlesden–Popper structure can accommodate a considerable amount of excess oxygen on interstitial sites[13] resulting in a high oxygen incorporation rate and high, but anisotropic, oxygen-ion conductivity.[14–17]

Studies investigating thin films from the $La_{n+1}Ni_nO_{3n+1}$ system have concentrated on films grown by physical vapor deposition (PVD),[1–3,18] metal organic chemical vapor deposition (MOCVD)[9] or nebulized spray pyrolysis.[8,19] These

* Corresponding author. Tel.: +41 44 632 71 56; fax: +41 44 632 11 32.
E-mail address: thomas.ryll@mat.ethz.ch (T. Ryll).

0955-2219/$ – see front matter © 2012 Elsevier Ltd. All rights reserved.
doi:10.1016/j.jeurceramsoc.2011.12.032

techniques conjointly yield epitaxial and dense microstructures. However, nanoporous microstructures featuring a high surface area are required for applications of thin films where reactions with a gas phase are essential, e.g. SOFC electrodes. In this regard deposition techniques based on organometallic precursor solutions, e.g. wet spray pyrolysis, have been proven to be well suited, rendering nanoporous and untextured thin films with equiaxed grains in the nanometer range at a high deposition rate and low cost.[20–23]

In this study, we demonstrate the applicability of wet spray pyrolysis for the deposition of ceramic thin films from the $La_{n+1}Ni_nO_{3n+1}$ system. The impact of crystallization and phase transformation on the microstructure and electronic conductivity of porous $LaNiO_{3-\delta}$ and $La_4Ni_3O_{10-\delta}$ thin films are presented. Furthermore, the performance of porous $LaNiO_{3-\delta}$ and $La_4Ni_3O_{10-\delta}$ thin films with respect to the oxygen reduction reaction on a $Ce_{0.8}Gd_{0.2}O_{1.9}$ (CGO) electrolyte is assessed.

2. Experimental

2.1. Preparation of thin films

Lanthanum nickelate thin films were deposited by air-pressurized spray pyrolysis on randomly oriented sapphire single crystals (Stettler, Switzerland) and polycrystalline $Ce_{0.8}Gd_{0.2}O_{1.9}$ (CGO) electrolyte pellets. A detailed description of the preparation of CGO electrolyte pellets can be found elsewhere.[24] The composition of the spray solution as well as the experimental parameters used during spray pyrolysis are specified in Table 1. During deposition the spray solution was pumped (syringe pump A99, Razel Scientific Instruments, USA) through a nozzle (Binks 460, J92P air nozzle, J920 fluid nozzle, Binks, USA) and atomized by air pressure. The substrate was positioned at a distance of 38 cm below the nozzle on a hot plate (CT 10, Harry Gestigkeit, Germany). Subsequent heat treatments at temperatures between 540 °C and 1100 °C were performed in air (L3, Nabertherm, Germany) using a dwell time of 4 h and a heating and cooling rate of 3 °C min^{-1}.

Table 1
Experimental parameters used for the deposition of thin lanthanum nickelate films by spray pyrolysis.

Substrate	Randomly oriented sapphire single crystals (α-Al_2O_3) (Stettler, Switzerland), polycrystalline $Ce_{0.8}Gd_{0.2}O_{1.9}$ (CGO) pellets
Salt mixture	50 mol% $La(NO_3)_3{\cdot}6H_2O$ (Fluka, Switzerland, purity ≥ 99 mol%) 50 mol% $Ni(NO_3)_2{\cdot}6H_2O$ (ABCR, Germany, purity ≥ 99.9 mol%)
Solvent composition	10 vol.% ethanol (Merck, USA, purity ≥ 99.9 vol.%, bp 78 °C, density 0.79 g cm^{-3}) 10 vol.% polyethylene glycol 600 (Fluka, Switzerland, bp 200 °C, density 1.21 g cm^{-3}) 80 vol.% diethylene glycol (Acros, Belgium, purity ≥ 99 vol.%, bp 245 °C, density 1.1 g cm^{-3})
Total salt concentration	0.05 mol/l
Substrate temperature	350 ± 5 °C, measured with a type K surface probe (Omega, Germany, Model 88108)
Air pressure	1 bar
Solution flow rate	5 ml/h
Spray time	30 min on Al_2O_3, 60 min on CGO

2.2. Structural and microstructural characterization

In order to analyze the crystallization and phase transformation behavior of lanthanum nickelate thin films, Differential Scanning Calorimetry (DSC) and Thermogravimetry (TG, both Netzsch STA 449 C Jupiter, Netzsch, Germany) were applied. 20 mg of film material were scratched off the Al_2O_3 substrate after 10 h of deposition. The resulting powder was investigated in a Pt crucible in air, using a heating and cooling rate of 20 °C min^{-1} up to a maximum temperature of 1350 °C.

The crystallinity and crystal structure of lanthanum nickelate thin films were investigated by Grazing Incidence X-ray Diffraction (GIXRD, XPert Pro MPD, Panalytical, Netherlands, Cu anode, 40 mA current, 45 kV acceleration voltage) using a parallel beam geometry and a fixed incidence angle of 1°. Reference peak positions were obtained by the web application of the Inorganic Crystal Structure Database (ICSD).[25] For the refinement of GIXRD patterns and the calculation of lattice parameters the software Maud was applied.[26,27]

The surface structure of lanthanum nickelate thin films was visualized by a Leo 1530 Scanning Electron Microscope (SEM, Carl Zeiss SMT, Germany). Images were recorded by an in-lens detector using an acceleration voltage of 3 kV. Cross-sections of thin films were cut, polished and imaged by a Focused Ion Beam (FIB) workstation (Nvision 40, Carl Zeiss SMT, Germany). For the quantitative analysis of SEM images with respect to grain size and porosity the software Lince 2.31 was applied.[28] The error margins of grain size and porosity were assessed by the analysis of images comprising a statistically significant number of features taken on two identically prepared samples in each case.

The elemental composition of lanthanum nickelate thin films was analyzed by Rutherford Backscattering Spectrometry (RBS) and Particle-Induced X-ray Emission (PIXE) using 2 MeV ^4He ions. RBS spectra were evaluated using the software RUMP.[29] Concentrations of impurity elements were calculated from the intensity ratios of K_α and L_α lines compared to the Ni K_α line in PIXE spectra using literature values for branching ratios, fluorescence yields and ionization cross-sections.[30,31]

2.3. Electrical and electrochemical characterization

For measurements of lateral DC conductivity, lanthanum nickelate films were deposited through a shadow mask (open area of 1.4 cm × 2.5 cm, 200 μm thick stainless steel) on sapphire single crystals. The films were contacted by four stripes of sputtered platinum, platinum paste (C 3605 S, Heraeus, Germany) and platinum wire. The wires fixed on the film surface by ceramic two-component cement (Feuerfestkitt,

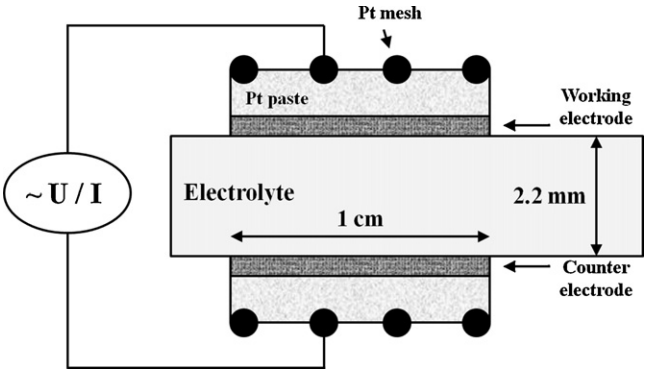

Fig. 1. Schematic cross-section of a symmetrical cell for the characterization of lanthanum nickelate thin films by electrochemical impedance spectroscopy.

Firag, Switzerland) were spot welded to wires connected to a multimeter (model 2700, Keithley, USA). Further details concerning the contacting approach are given elsewhere.[23] Conductivity measurements were conducted on a hot plate (CT10, Harry Gestigkeit, Germany) during cooling at a rate of 3 °C min^{-1}. Within the error estimation of conductivity, systematic errors resulting from the uncertainty with respect to sample geometry and thickness as well as statistical errors assessed by several measurements using at least two identical samples were considered.

Impedance data were measured on symmetrical cells fabricated by the deposition of one square centimeter of thin film area symmetrically on both sides of CGO electrolyte pellets (Fig. 1). For the contacting of thin films platinum paste (C 3605 S, Heraeus, Germany) and flattened platinum mesh (52 mesh, woven from wires with a diameter of 0.1 mm, Johnson Matthey, UK) were used. A detailed description of the film contacting approach is given elsewhere.[24] Symmetrical cells were mounted in a tube furnace (Gero, Germany) constantly flushed by 50 ml min^{-1} of humidified air. Measurements were done during stepwise cooling from the maximum temperature. At each temperature step 10 min were awaited isothermally to let the sample equilibrate. In order to monitor the temperature a thermocouple (Omega, USA) was placed next to the sample. Electrochemical impedance spectroscopy was performed using a SI 1260 impedance bridge (Solartron, UK), operated between 1 mHz and 4 mHz using an oscillation amplitude of 20 mV. Exemplary impedance spectra measured at 550 °C and 600 °C are shown in Fig. 2A. Impedance spectra were analyzed and fitted by the equivalent circuit shown in Fig. 2B using the software ZView 2.9c.[32] Two semicircles could be distinguished. High frequency arcs were attributed to the electrolyte on the basis of relaxation times, their independence on an applied DC bias and comparison of the resulting conductivity values with literature data. By means of capacitance values and relaxation times the low frequency impedance features were ascribed to the electrode process and the corresponding ohmic resistance to the electrode polarization resistance. Due to the characterization of symmetrical cells, area specific resistances (*ASRs*) were obtained by multiplication of half of the electrode polarization resistance by the electrode area.

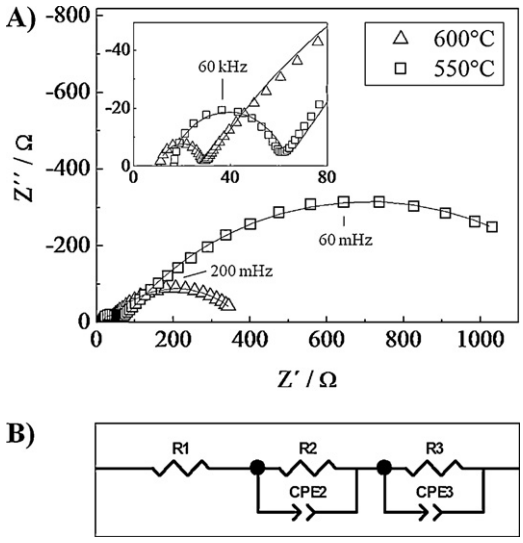

Fig. 2. (A) Impedance spectra of a symmetrical cell comprising a lanthanum nickelate thin film on a CGO pellet. The high frequency region is magnified in the inset. The discrete data points represent the original impedance data while the continuous line corresponds to the resulting fit. (B) Equivalent circuit used for the fitting of impedance data. R and CPE refer to ohmic resistances and constant phase elements, respectively.

3. Results and discussion

3.1. Crystallization

During heating, metal oxide thin films deposited by precipitation-based techniques like spray pyrolysis undergo major changes including the evaporation of residual organic solvents and hydroxyl water, crystallization as well as phase transformations of the thin film material. DSC and TG have been shown to be useful techniques for the investigation of such processes.[33]

In Fig. 3 the evolution of heat and mass of as-deposited thin film material during the first heat-up to 1350 °C are plotted. A major mass loss of 15.5 wt.% occurs between the deposition temperature of 350 °C and 800 °C. In agreement with literature

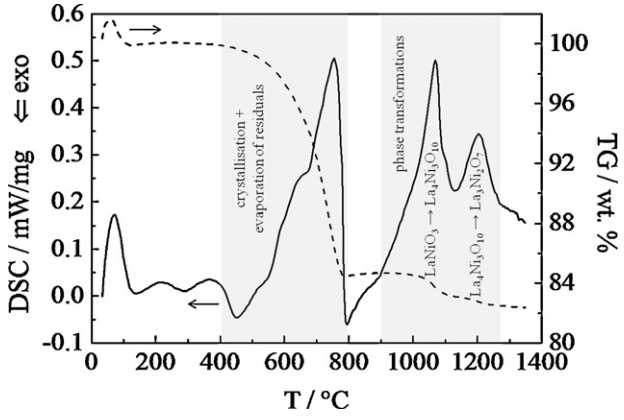

Fig. 3. Evolution of heat and weight loss of lanthanum nickelate film material transforming from the amorphous to the crystalline state and subsequently decomposing into $La_4Ni_3O_{10-\delta}$ and $La_3Ni_2O_{7-\delta}$ at 1052 °C and 1171 °C, corresponding to the reactions (1) and (2), respectively.

this loss is attributed to the removal of gaseous species tracing back to the organic solvents in the spray solution and hydroxyl groups.[23,33] The concurrent volumetric loss between 350 °C and 800 °C is estimated to add up to 54 vol.%, provided that (i) the density of the organic residues in the as-deposited lanthanum nickelate thin films corresponds to the mean density of the spray solution (1.09 g cm^{-3}) and (ii) the density of as-deposited lanthanum nickelate is close to the density of crystalline $LaNiO_{3-\delta}$ (7.09 g cm^{-3} [2]). Around 400 °C, the DSC signal exhibits the onset of an exothermal minimum that passes into a large endothermal peak with a maximum value at 750 °C. Based on the above-mentioned mass loss the endothermal peak is attributed to the removal of gaseous species and most likely superimposes an exothermal crystallization maximum. Further mass losses of 1.6 wt.% and 0.7 wt.% in conjunction with distinct endothermal DSC maxima occur around 1069 °C and 1204 °C, respectively. In DSC experiments involving heating of the $LaNiO_{3-\delta}$ compound in an oxygen partial pressure of 0.1 bar with 10 °C min^{-1}, literature reports endothermal DSC maxima at 1052 °C and 1171 °C corresponding to the decomposition reactions of the Ruddlesden–Popper phases (1) and (2).[10] The theoretical mass losses due to oxygen formation during the two reactions are 1.63 wt.% and 0.60 wt.%, respectively. Based on the agreement of these values with the mass losses and temperatures of the DSC maxima found in this study, the two endothermal reactions are likewise attributed to the stepwise thermal decomposition reactions (1) and (2) of the Ruddlesden–Popper phases. The slightly higher temperatures of DSC maxima compared to literature data result from the higher heating rate (20 °C min^{-1}) and atmospheric oxygen partial pressure applied during the DSC measurements. Given that no temperatures higher than 1350 °C were applied in the DSC experiments shown in this study, the final reaction (3) resulting in the compound $La_2NiO_{4+\delta}$ was not observed.

Based on the DSC/TG results, annealing temperatures of 540 °C, 660 °C and 800 °C covering the temperature range of solvent evaporation and crystallization, and 1100 °C resulting in the $La_4Ni_3O_{10-\delta}$ phase were chosen for further experiments.

GIXRD patterns of as-deposited and annealed lanthanum nickelate thin films are shown in Fig. 4. The GIXRD patterns of as-deposited lanthanum nickelate films contain primarily peaks resulting from the CGO substrate. Three minor reflections around 27°, 45° and 54° can neither be assigned to any known lanthanum nickelate phase, ceria phase nor any potential reaction product of the thin film and the electrolyte. However, these peaks do not appear in GIXRD patterns of as-deposited lanthanum nickelate films on Al_2O_3 single crystals, for which reason they most likely trace back to some minor foreign phase in the CGO electrolyte. Hence, GIXRD confirms that as-deposited lanthanum nickelate thin films are amorphous.

After annealing at 540 °C, 660 °C and 800 °C GIXRD patterns comprise additional peaks that are assigned to the rhombohedral perovskite $LaNiO_{3-\delta}$ with space symmetry R-3 m.[6] Accordingly, amorphous lanthanum nickelate thin films deposited by spray pyrolysis begin to crystallize between 350 °C and 540 °C. This substantiates the assumption that the exothermal DSC minimum starting at 400 °C represents the

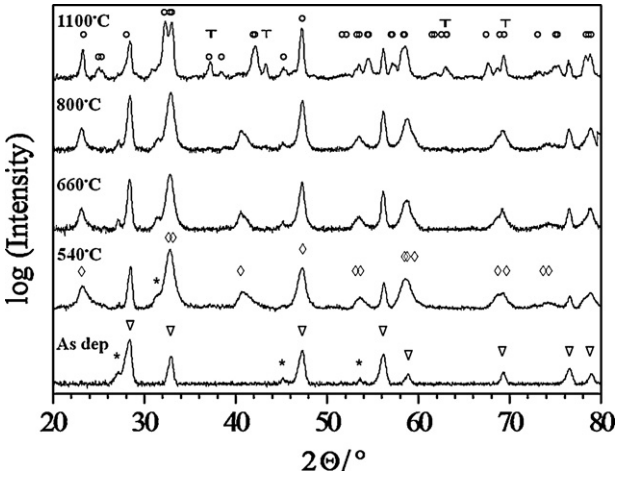

Fig. 4. GIXRD patterns of lanthanum nickelate films deposited on CGO electrolyte pellets by spray pyrolysis. Samples were heat treated for 4 h at different temperatures in air. Reference peak positions for $LaNiO_{3-\delta}$ (◊,[34]), $La_4Ni_3O_{10}$ (◯,[47]), NiO (⊤,[48]) and $Ce_{0.8}Gd_{0.2}O_{1.9}$ (▽,[49]) as well as unassigned reflections (*) are marked. Single phase $LaNiO_{3-\delta}$ prevails up to 800 °C whereas multiple phases ($LaNiO_{3-\delta}$, $La_4Ni_3O_{10}$ and NiO) occur at higher temperatures.

crystallization of the thin film material. The refinement of the spectrum measured after annealing at 660 °C renders lattice parameters of $a = 5.45$ Å and $c = 13.15$ Å which are in accordance with literature for bulk ceramics.[34–36] The diffraction lines in GIXRD patterns recorded after annealing at 1100 °C are attributed to the Ruddlesden–Popper phase $La_4Ni_3O_{10-\delta}$ and NiO. This finding is in accordance with the DSC/TG results and confirms the endothermal decomposition of $LaNiO_{3-\delta}$ thin films around 1052 °C according to reaction (1). Lanthanum nickelate thin films heat treated at temperatures exceeding 1100 °C exhibit reactions with the substrate and were therefore excluded from this study. As the GIXRD reflections attributed to $LaNiO_{3-\delta}$ and $La_4Ni_3O_{10-\delta}$ appear in the expected intensity ratio, no indication for a preferred grain orientation is found. This is in contrast to studies where the deposition of thin films from the $La_{n+1}Ni_nO_{3n+1}$ series by nebulized spray pyrolysis gave rise to pronounced texturing.[8,19] The reason for this significant microstructural difference, despite the use of a similar deposition technique, is a different ratio of the substrate temperature during deposition T_s and the boiling point of the organic solvent in the precursor solution T_{bp}. The value $T_s/T_{bp} > 5$ used in[8,19] involves complete evaporation of the solvent on the way to the substrate. Accordingly, nucleation occurs from the gas phase resulting in layer-by-layer-like growth and the formation of a preferred grain orientation. By contrast, the value of $T_s/T_{bp} = 1.6$ used in this study leads to the arrival of liquid droplets on the substrate surface and precipitation of three-dimensional nuclei of amorphous film material.[37] The resulting amorphous matrix transforms into a microstructure without a preferred grain orientation during crystallization. More information on wet spray pyrolysis is available in literature.[38] A similar lack of a preferred orientation has also been observed for thin $LaNiO_{3-\delta}$ films deposited by spin coating of a polymeric precursor solution containing lanthanum and nickel salts.[39]

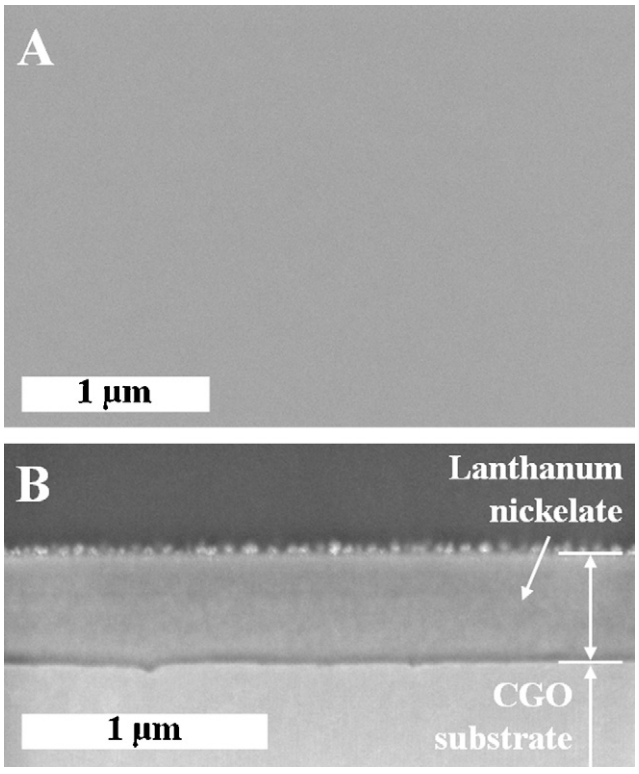

Fig. 5. Microstructure of amorphous lanthanum nickelate films after deposition on polycrystalline CGO electrolyte pellets by spray pyrolysis. (A) Top-view and (B) FIB-cut cross-section.

It can be concluded that as-deposited lanthanum nickelate thin films fabricated by spray pyrolysis are amorphous. Crystallization starts at 400 °C, whereas the removal of gaseous species originating from the organic solvents in the spray solution and hydroxyl groups continues until 800 °C. This outgassing during crystallization causes a volumetric loss of 54 vol.% compared to the as-deposited state. The perovskite $LaNiO_{3-\delta}$ that was found to form up to 800 °C decomposes into the Ruddlesden–Popper phase $La_4Ni_3O_{10-\delta}$ around 1052 °C.

3.2. Microstructure

SEM images of lanthanum nickelate films after deposition by spray pyrolysis on polycrystalline CGO electrolyte pellets are shown in Fig. 5. As-deposited, amorphous films are dense, smooth and free from cracks. 60 min of deposition result in a film thickness around 350 nm and a corresponding deposition rate of 5.8 nm min^{-1}.

The microstructure of lanthanum nickelate films annealed at different temperatures for 4 h is displayed in Fig. 6. Corresponding values of grain size and porosity are plotted in Fig. 7. Thin $LaNiO_{3-\delta}$ films annealed at 540 °C (compare Fig. 6A and B) exhibit equiaxed grains with a diameter of 37(7) nm, an equally distributed porosity adding up to 26(1) vol.% and an overall film thickness around 250 nm. An increase of the annealing temperature to 660 °C and 800 °C involves a roughly linear increase of the grain size, whereas the porosity stays constant considering the error margins of the porosity values. In literature, similar microstructures have been observed after the deposition of $LaNiO_{3-\delta}$ thin films by repeated spin coating of an organometallic solution and adjacent annealing.[21] Comparing the cross-sections shown in Fig. 6B, D and F, it becomes apparent that the grain growth is accompanied by a decrease of the contact area between the $LaNiO_{3-\delta}$ films and the CGO electrolyte. $LaNiO_{3-\delta}$ films annealed at 800 °C are approximately 200 nm thick. In consideration of the porosity, this film thickness corresponds to a volumetric loss of 58 vol.% compared to the as-deposited films. This value matches the 54 vol.%, estimated on the basis of TG measurements. Accordingly, the removal of gaseous species gives rise to pore formation and the reduction of film thickness during annealing.

As shown in Fig. 6G, thin $La_4Ni_3O_{10}$ films annealed at 1100 °C exhibit a dense film surface and a mean grain diameter of 350(60) nm. In FIB-cut cross sections (Fig. 6H) isolated pores at the interface between the film and the CGO electrolyte resulting in a porosity of 14(5) vol.% are observed. In contrary to the $LaNiO_{3-\delta}$ films annealed between 540 °C and 800 °C, $La_4Ni_3O_{10-\delta}$ films comprise one layer of laterally connected grains in close contact with the CGO electrolyte. The significantly higher grain size and lower porosity of $La_4Ni_3O_{10-\delta}$ film compared to $LaNiO_{3-\delta}$ films are attributed to sintering processes caused by the comparatively high temperature of 1100 °C which is required to obtain the $La_4Ni_3O_{10-\delta}$ phase.

3.3. Elemental composition

The elemental composition of $LaNiO_{3-\delta}$ films on sapphire substrates annealed at 660 °C for 4 h was analyzed by RBS and PIXE. The evaluation of the RBS spectrum shown in Fig. 8A yields a La:Ni ratio of 1:1. Besides La and Ni the corresponding PIXE spectrum shown in Fig. 8B points at the presence of impurity elements. Whereas the atomic percentage of S, Pd, Ru and K compared to the total amount of cations is between 0.1 and 0.2 at.%, the amount of Gd and Sc adds up to 0.7 and 2.0 at.%, respectively. It is assumed that the detected impurity elements originate either from the lanthanum and nickelate salts dissolved in the spray solution or from the spray setup. While traces of impurities can hardly be avoided, their quantification is important in order to facilitate the comparison of electrical and electrochemical properties with literature data.

3.4. Electrical conductivity

The electrical conductivity of lanthanum nickelate thin films annealed at different temperatures is plotted in Fig. 9. In order to avoid the distortion of conductivity values by a conductive substrate, thin films deposited on insulating sapphire crystals were used for conductivity measurements.

During the first heating as-deposited films exhibit a low but strongly thermally activated conductivity. As long as the crystallization temperature of 400 °C is not exceeded, this behavior is retained during further heating and cooling cycles. The electrical conductivity of $LaNiO_{3-\delta}$ films annealed at 540 °C is around 490 S cm^{-1} at room temperature and exhibits a metal-type temperature dependence. These characteristics correspond well with

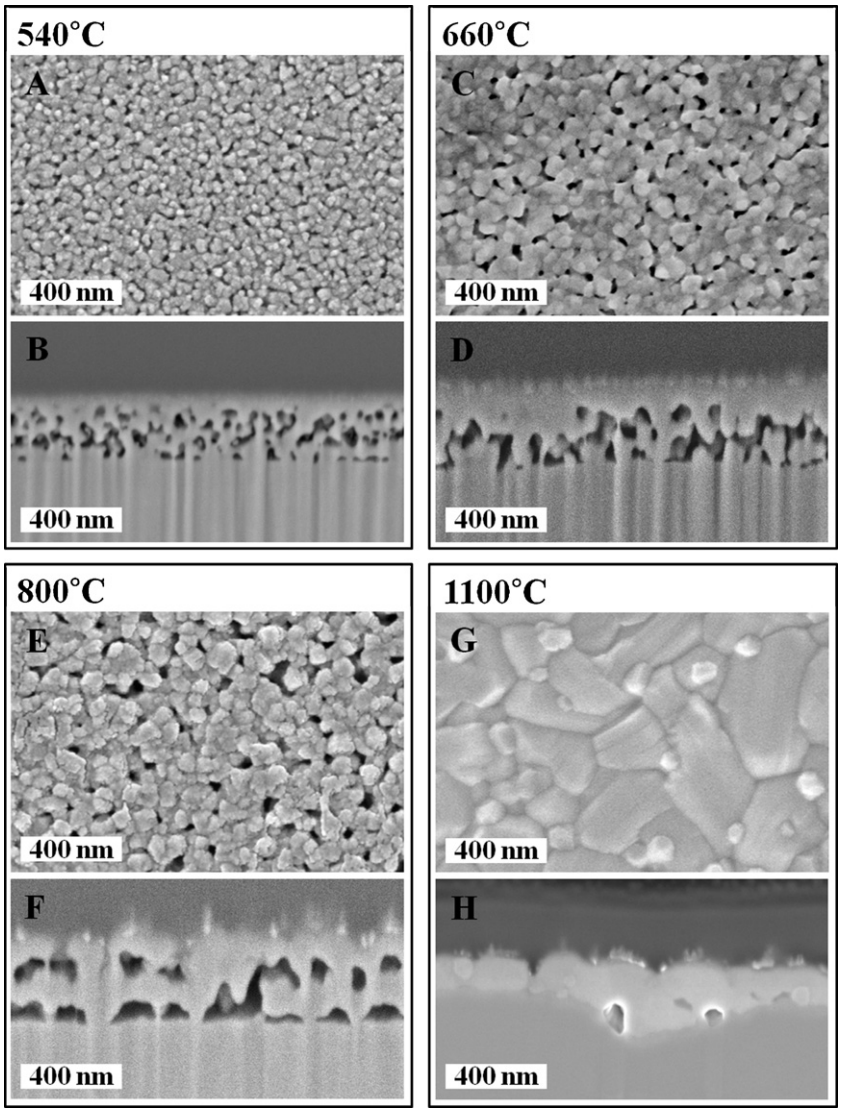

Fig. 6. Microstructure of crystalline lanthanum nickelate films on polycrystalline CGO electrolyte pellets obtained after annealing for 4 h at different temperatures in air. (A–F) $LaNiO_{3-\delta}$; (G–H) $La_4Ni_3O_{10-\delta}$.

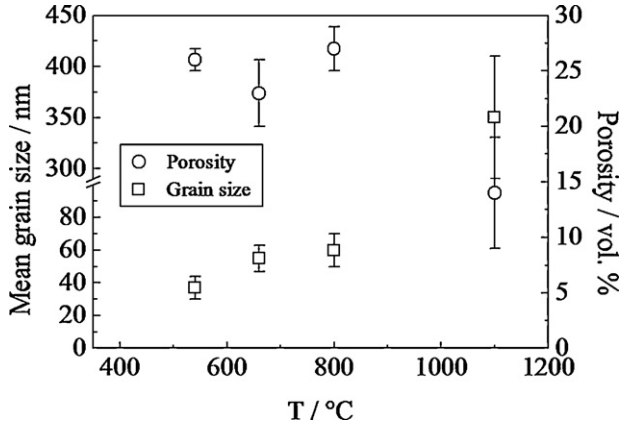

Fig. 7. Grain size and porosity of lanthanum nickelate films deposited on polycrystalline CGO electrolyte pellets and annealed for 4 h at different temperatures in air.

literature, even though the exceptionally high conductivity of $LaNiO_{3-\delta}$ films presented by Burriel et al.[9] is not reached. An increase of the annealing temperature results in a stepwise increase of the electrical conductivity up to 1220 S cm^{-1} at room temperature after annealing at 800 °C. We assume that this increase results from a decreasing scattering of charge carriers at residues tracing back to the organic solvents and grain boundaries with increasing annealing temperature and grain size. The overall increase of electrical conductivity with increasing annealing temperature does not impact the metallic conduction characteristics of the $LaNiO_{3-\delta}$ films investigated in this study. $La_4Ni_3O_{10-\delta}$ thin films annealed at 1100 °C exhibit a slightly thermally activated conductivity which is approximately one order of magnitude lower compared to $LaNiO_{3-\delta}$ films. While the overall magnitude of conductivity corresponds well with literature, the Ruddlesden–Popper phase $La_4Ni_3O_{10-\delta}$ has been reported to exhibit a metal-type temperature dependence of conductivity.[4–6,40–42] This disagreement might result from the

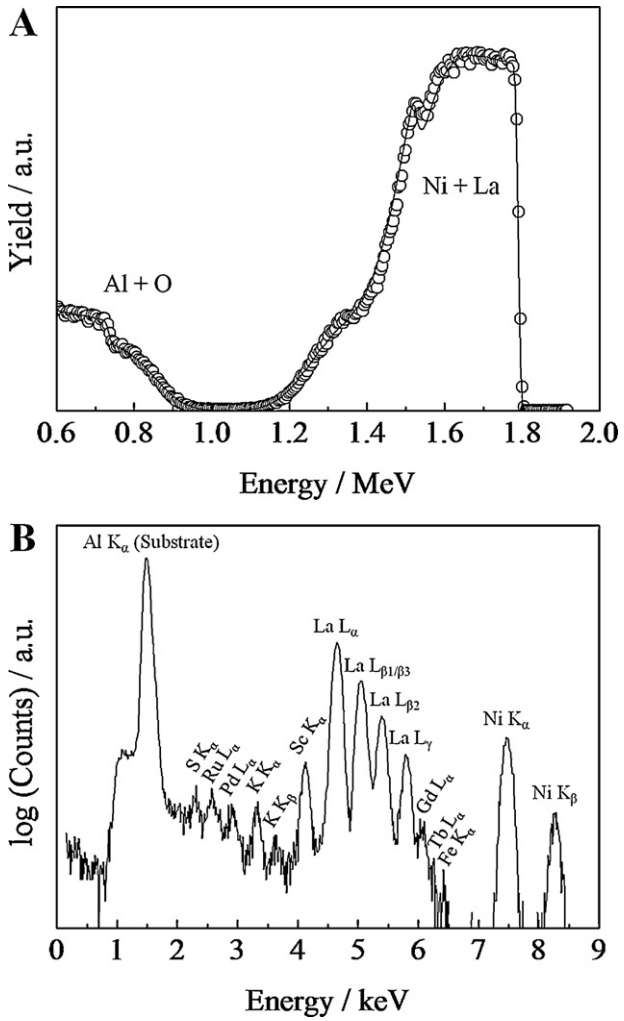

Fig. 8. Results of Rutherford Backscattering Spectrometry (RBS) measurements on a $LaNiO_{3-\delta}$ film on sapphire, annealed for 4 h at 660 °C in air. (A) RBS data (◯) and simulated spectrum (continuous line) and (B) corresponding PIXE spectrum.

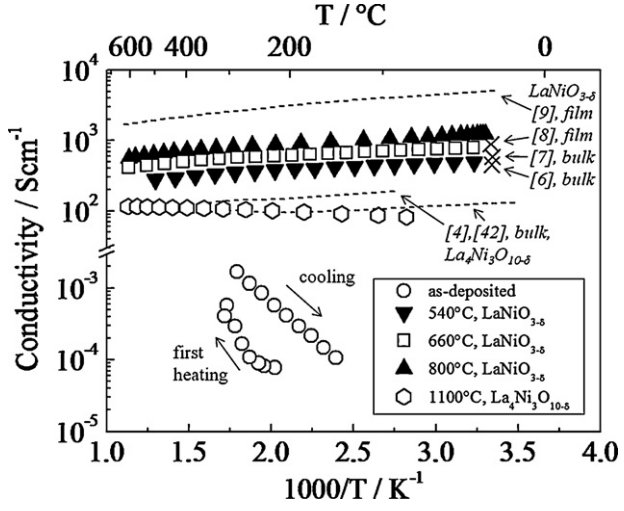

Fig. 9. Electrical conductivity of lanthanum nickelate films on sapphire. The films were annealed for 4 h at different temperatures in air. Errors do not exceed the size of the symbols. For comparison literature data for $LaNiO_{3-\delta}$ and $La_4Ni_3O_{10-\delta}$ samples is plotted as well.

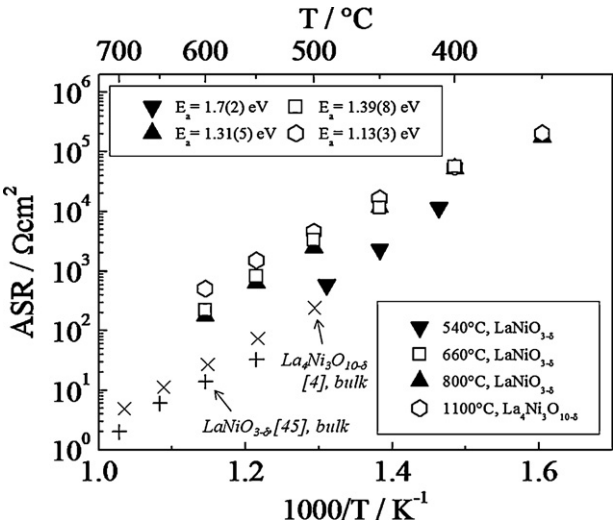

Fig. 10. Electrochemical performance of lanthanum nickelate films on CGO annealed for 4 h at different temperatures in air. For comparison literature data for $LaNiO_{3-\delta}$ and $La_4Ni_3O_{10-\delta}$ samples is plotted as well.

incorporation of 2 at.% of the larger impurity ion Sc^{3+} on $Ni^{2+/3+}$ sites, as detected by PIXE measurements. A comparable transition from metallic to semiconducting behavior was observed after the substitution of Ni in $LaNiO_{3-\delta}$ by Co or Ti.[43,44]

Summing up, both $LaNiO_{3-\delta}$ and $La_4Ni_3O_{10-\delta}$ thin films fabricated in this study exhibit electrical conductivities above 80 S cm^{-1} in the temperature range between room temperature and 600 °C. The observed magnitudes of conductivities correspond with literature data and are adequate for electrode applications.

3.5. Electrochemical performance

The electrochemical performance of lanthanum nickelate thin films on CGO annealed at different temperatures was investigated by electrochemical impedance spectroscopy. The resulting *ASRs* are plotted in Fig. 10. $LaNiO_{3-\delta}$ films annealed at 540 °C exhibit an *ASR* of 0.59 kΩ cm^2 at 500 °C, whereas annealing at 660 °C and 800 °C results in *ASRs* around 3 kΩ cm^2. It is interesting to note that, in contrast to the electronic conductivity, the presence of organic remains and hydroxyl groups as well as a potential partial crystallinity promote the cathode performance of $LaNiO_{3-\delta}$ thin films. In addition, the lower grain and pore size of samples annealed at 540 °C may contribute to the higher cathode performance compared to samples annealed at 660 °C and 800 °C. The activation energy for the cathode process in case of thin films annealed at 660 °C and 800 °C is 1.39(8) eV and 1.31(5) eV, respectively. This value corresponds reasonably well with literature data for thick $LaNiO_{3-\delta}$ films on CGO.[45] By contrast, the overall *ASR* of $LaNiO_{3-\delta}$ films annealed at 660 °C and 800 °C exceeds the literature data by more than one order of magnitude. The reason for this mismatch might be the decreasing contact area between thin film cathode and electrolyte observable in the cross-sections shown in Fig. 6. The *ASR* of $La_4Ni_3O_{10-\delta}$ thin films annealed at 1100 °C adds up to 16.5 kΩ cm^2 at 500 °C and exhibits an activation energy of

1.13(3) eV. In literature *ASR* values of $La_4Ni_3O_{10-\delta}$ thick films on a $La_{0.9}Sr_{0.1}Ga_{0.8}Mg_{0.2}O_{3-\delta}$ (LSGM) electrolyte have been reported that are one order of magnitude lower compared to the values measured in this study.[4] This difference might trace back on the one hand to the different choice of substrate material, as it has been shown that the *ASR* of lanthanum nickelate based cathodes on LSGM is more than two orders of magnitude lower compared to the same film on CGO.[46] On the other hand the closed surface, low porosity and relatively high grain size of the $La_4Ni_3O_{10-\delta}$ films annealed at 1100 °C do not provide a promising microstructural basis for high cathode performances. Further studies have to clarify whether the $La_4Ni_3O_{10-\delta}$ phase is accessible in thin films deposited by spray pyrolysis without annealing at high temperatures. Directions in this regard are given by studies where $La_4Ni_3O_{10-\delta}$ films were obtained by nebulized spray pyrolysis[8,19] or MOCVD[9] after an appropriate choice of the La/Ni ratio in the precursor solution.

It is acknowledged that the *ASR* values measured in this study are comparably high. Further microstructural optimization is required in order to make use of the promising oxygen incorporation and oxygen conduction properties of thin films from the $La_{n+1}Ni_nO_{3n+1}$ system.

4. Conclusions

Thin lanthanum nickelate films deposited on sapphire and CGO substrates by spray pyrolysis are amorphous. After spray deposition, both crystal structure and microstructure of thin films from the $La_{n+1}Ni_nO_{3n+1}$ system can be tailored by heat treatments: by annealing between 540 °C and 800 °C rhombohedral $LaNiO_{3-\delta}$ films with equiaxed grains in the 50 nm range and a porosity around 25 vol.% are obtained. Grain and pore size increase with rising annealing temperature. Simultaneously, the metallic conductivity of $LaNiO_{3-\delta}$ films increases due to the removal of organic remains. Commensurate with the phase diagram, thin $La_4Ni_3O_{10-\delta}$ films with Ruddlesden–Popper structure are obtained after annealing at 1100 °C. $La_4Ni_3O_{10-\delta}$ films exhibit a dense microstructure with grains in the range of 350 nm and are found to be semiconducting in the temperature range between room temperature and 600 °C.

$LaNiO_{3-\delta}$ and $La_4Ni_3O_{10-\delta}$ thin films deposited by spray pyrolysis qualify for electrode applications due to their high electrical conductivity above 80 S cm^{-1} between room temperature and 600 °C. However, the *ASR* values, measured on a CGO electrolyte in air, have been found to suffer from a decreasing contact area between electrode and electrolyte with increasing annealing temperature in case of $LaNiO_{3-\delta}$ layers, and a dense microstructure with large grains in case of $La_4Ni_3O_{10-\delta}$ films. Microstructural improvements are required in order to enhance the cathode performance of sprayed $LaNiO_{3-\delta}$ and $La_4Ni_3O_{10-\delta}$ thin films.

Acknowledgments

Financial assistance by the following Swiss institutions is gratefully acknowledged: (i) Competence Centre for Materials Science and Technology (CCMX) within the framework of the NANCER project; (ii) Center of Competence Energy and Mobility (CCEM) within the framework of the ONEBAT project; (iii) Swiss Electric Research (SER) within the framework of the ONEBAT project; (iv) Swiss National Foundation (SNF) within the framework of the Sinergia project ONEBAT

References

1. Satyalakshmi KM, Mallya RM, Ramanathan KV, Wu XD, Brainard B, Gautier DC, et al. Epitaxial metallic $LaNiO_3$ thin-films grown by pulsed laser deposition. *Appl Phys Lett* 1993;**62**:1233–5.
2. Lee HY, Hsu CH, Hsieh YW, Chen YH, Liang YC, Wu TB, et al. Preparation of heteroepitaxial $LaNiO_3$ thin films on a $SrTiO_3$ substrate for growing an artificial superlattice with RF sputtering. *Mater Chem Phys* 2005;**92**:585–90.
3. Zhao S, Ma F, Song ZX, Xu KW. The growth behavior and stress evolution of sputtering-deposited $LaNiO_3$ thin films. *Mater Sci Eng A: Struct* 2008;**474**:134–9.
4. Amow G, Davidson IJ, Skinner SJ. A comparative study of the Ruddlesden–Popper series, $La_{n+1}Ni_nO_{3n+1}$ ($n = 1$, 2 and 3), for solid-oxide fuel-cell cathode applications. *Solid State Ionics* 2006;**177**:1205–10.
5. Takahashi S, Nishimoto S, Matsuda M, Miyake M. Electrode properties of the Ruddlesden–Popper series, $La_{n+1}Ni_nO_{3n+1}$ ($n = 1$, 2, and 3), as intermediate-temperature solid oxide fuel cells. *J Am Ceram Soc* 2010;**93**:2329–33.
6. Sreedhar K, McElfresh M, Perry D, Kim D, Metcalf P, Honig JM. Low-temperature electronic properties of the $La(n+1)Ni(n)O(3n+1)$ ($n = 2$, 3, and infinity) system – evidence for a crossover from fluctuating-valence to fermi-liquid-like behavior. *J Solid State Chem* 1994;**110**:208–15.
7. Ram MRA, Ganapathi L, Ganguly P, Rao CNR. Evolution of three-dimensional character across the $La_{n+1}Ni_nO_{3n+1}$ homologous series with increase in *n*. *J Solid State Chem* 1986;**63**:139–47.
8. Raju AR, Aiyer HN, Rao CNR. Oriented films of $LaNiO_3$ and other members of the $La_{n+1}Ni_nO_{3n+1}$ series, $LaCuO_{3-\delta}$ and Pb(Zr0.52Tl0.48)O-3, obtained by nebulized spray pyrolysis. *Chem Mater* 1995;**7**:225–31.
9. Burriel M, Garcia G, Rossell MD, Figueras A, Van Tendeloo G, Santiso J. Enhanced high-temperature electronic transport properties in nanostructured epitaxial thin films of the $La_{n+1}Ni_nO_{3n+1}$ Ruddlesden–Popper series ($n = 1$, 2, 3, infinity). *Chem Mater* 2007;**19**:4056–62.
10. Zinkevich M, Solak N, Nitsche H, Ahrens M, Aldinger F. Stability and thermodynamic functions of lanthanum nickelates. *J Alloys Compd* 2007;**438**:92–9.
11. Zinkevich M, Aldinger F. Thermodynamic analysis of the ternary La–Ni–O system. *J Alloys Compd* 2004;**375**:147–61.
12. Drennan J, Tavares CP, Steele BCH. An electron-microscope investigation of phases in the system La–Ni–O. *Mater Res Bull* 1982;**17**:621–6.
13. Jorgensen JD, Dabrowski B, Pei S, Richards DR, Hinks DG. Structure of the interstitial oxygen defect in $La_2NiO_{4+\delta}$. *Phys Rev B* 1989;**40**:2187–99.
14. Kharton VV, Viskup AP, Naumovich EN, Marques FMB. Oxygen ion transport in La_2NiO_4-based ceramics. *J Mater Chem* 1999;**9**:2623–9.
15. Boehm E, Bassat JM, Steil MC, Dordor P, Mauvy F, Grenier JC. Oxygen transport properties of $La_2Ni_{1-x}Cu_xO_{4+\delta}$ mixed conducting oxides. *Solid State Sci* 2003;**5**:973–81.
16. Minervini L, Grimes RW, Kilner JA, Sickafus KE. Oxygen migration in $La_2NiO_{4+\delta}$. *J Mater Chem* 2000;**10**:2349–54.
17. Bassat JM, Odier P, Villesuzanne A, Marin C, Pouchard M. Anisotropic ionic transport properties in $La_2NiO_{4+\delta}$ single crystals. *Solid State Ionics* 2004;**167**:341–7.
18. Briois P, Perry F, Billard A. Structural and electrical characterisation of lanthanum nickelate reactively sputter-deposited thin films. *Thin Solid Films* 2008;**516**:3282–6.
19. Aiyer HN, Raju AR, Subbanna GN, Rao CNR. Epitaxial nature of the films of $LaNiO_3$, Pb(Zr0.5Ti0.5)O-3, and La0.95Mn0.95O_3 obtained by nebulized spray pyrolysis. *Chem Mater* 1997;**9**:755–60.
20. Hwang KS, Min SS, Park YJ. Formation of highly-oriented and polycrystalline lanthanum nickelate films by a spin coating-pyrolysis process. *Surf Coat Technol* 2001;**137**:205–8.

21. Wu GH, Ruan KB, Liang T, Chen XM, Bao DH. Preparation and conductive properties of neodymium-doped lanthanum nickelate thin films by chemical solution deposition method. *Thin Solid Films* 2009;**517**:1563–6.
22. Patil PS. Versatility of chemical spray pyrolysis technique. *Mater Chem Phys* 1999;**59**:185–98.
23. Beckel D, Dubach A, Grundy AN, Infortuna A, Gauckler LJ. Solid-state dewetting of La0.6Sr0.4Co0.2Fe0.8$O_{3\pm\delta}$ thin films during annealing. *J Eur Ceram Soc* 2008;**28**:49–60.
24. Beckel D, Muecke UP, Gyger T, Florey G, Infortuna A, Gauckler LJ. Electrochemical performance of LSCF based thin film cathodes prepared by spray pyrolysis. *Solid State Ionics* 2007;**178**:407–15.
25. Bergerhoff G. Data-base for inorganic crystal-structures. *Comput Phys Commun* 1984;**33**:79–84.
26. Lutterotti L, Chateigner D, Ferrari S, Ricote J. Texture, residual stress and structural analysis of thin films using a combined X-ray analysis. *Thin Solid Films* 2004;**450**:34–41.
27. Lutterotti L. Total pattern fitting for the combined size-strain–stress-texture determination in thin film diffraction. *Nucl Instrum Meth B* 2010;**268**:334–40.
28. dos Santos e Lucato SL. *Lince v2. 31*. Darmstadt, Germany: Department of Materials Science, Darmstadt University of Technology; 1999. Lince-linear intercept v2.31.
29. Doolittle LR. A semiautomatic algorithm for Rutherford backscattering analysis. *Nucl Instrum Meth B* 1986;**15**:227–31.
30. LBNL Isotopes Project Nuclear Data Dissemination Home Page, http://ie.lbl.gov/toi.html; 2005.
31. Cohen DD, Harrigan M. Calculated l-shell X-ray-line intensities for proton and helium ion impact. *At Data Nucl Data Tables* 1986;**34**:393–414.
32. Johnson D. *ZView 2. 9c*. Scribner Associates, Inc. ZView 2.9c; 2005.
33. Rupp JLM, Scherrer B, Harvey A, Gauckler LJ. Crystallization and grain growth kinetics for precipitation-based ceramics: a case study on amorphous ceria thin films from spray pyrolysis. *Adv Funct Mater* 2009;**19**:9.
34. Garciamunoz JL, Rodriguezcarvajal J, Lacorre P, Torrance JB. Neutron-diffraction study of RNiO3 (R = La, Pr, Nd, Sm) – electronically induced structural changes across the metal–insulator transition. *Phys Rev B* 1992;**46**:4414–25.
35. Park JC, Kim DK, Byeon SH, Kim D. XANES study on Ruddlesden–Popper phase, $La_{n+1}Ni_nO_{3n+1}$ ($n = 1$, 2 and infinity). *J Synchrotron Radiat* 2001;**8**:704–6.
36. Yang J. Structural analysis of perovskite $LaCr_{1-x}Ni_xO_3$ by Rietveld refinement of X-ray powder diffraction data. *Acta Crystallogr B* 2008;**64**:281–6.
37. Perednis D, Gauckler LJ. Thin film deposition using spray pyrolysis. *J Electroceram* 2005;**14**:103–11.
38. Beckel D, Dubach A, Studart AR, Gauckler LJ. Spray pyrolysis of La0.6Sr0.4Co0.2Fe0.8$O_{3-\delta}$ thin film cathodes. *J Electroceram* 2006;**16**:221–8.
39. Escote MT, Pontes FM, Leite ER, Varela JA, Jardim RF, Longo E. Microstructural and transport properties of $LaNiO_{3-\delta}$ films grown on Si (1 1 1) by chemical solution deposition. *Thin Solid Films* 2003;**445**:54–8.
40. Zhang Z, Greenblatt M. Synthesis, structure, and properties of Ln(4)Ni(3)O(10-delta) (Ln = La, Pr, and Nd). *J Solid State Chem* 1995;**117**:236–46.
41. Bannikov DO, Cherepanov VA. Thermodynamic properties of complex oxides in the La–Ni–O system. *J Solid State Chem* 2006;**179**:2721–7.
42. Kobayashi Y, Taniguchi S, Kasai M, Sato M, Nishioka T, Kontani M. Transport and magnetic properties of $La_3Ni_2O_{7-\delta}$ and $La_4Ni_3O_{10-\delta}$. *J Phys Soc Jpn* 1996;**65**:3978–82.
43. Hrovat M, Katsarakis N, Reichmann K, Bernik S, Kuscer D, Holc J. Characterisation of $LaNi_{1-x}Co_xO_3$ as a possible SOFC cathode material. *Solid State Ionics* 1996;**83**:99–105.
44. Rodríguez E, Álvarez I, López ML, Veiga ML, Pico C. Structural, electronic, and magnetic characterization of the perovskite $LaNi_{1-x}Ti_xO_3$ ($0 < x < 1/2$). *J Solid State Chem* 1999;**148**:479–86.
45. Ralph JM, Schoeler AC, Krumpelt M. Materials for lower temperature solid oxide fuel cells. *J Mater Sci* 2001;**36**:1161–72.
46. Amow G, Skinner SJ. Recent developments in Ruddlesden–Popper nickelate systems for solid oxide fuel cell cathodes. *J Solid State Electrochem* 2006;**10**:538–46.
47. Voronin VI, Berger IF, Cherepanov VA, Gavrilova LY, Petrov AN, Ancharov AI, et al. Neutron diffraction, synchrotron radiation and EXAFS spectroscopy study of crystal structure peculiarities of the lanthanum nickelates $La_{n+1}Ni_nO_y$ ($n = 1$, 2, 3). *Nucl Instrum Meth A* 2001;**470**:202–9.
48. Rodic D, Spasojevic V, Kusigerski V, Tellgren R, Rundlof H. Magnetic ordering in polycrystalline $Ni_xZn_{1-x}O$ solid solutions. *Phys Status Solidi B* 2000;**218**:527–36.
49. Brauer G, Gradinger H. Ueber heterotype Mischphasen bei Seltenerdoxyden 1. *Z Anorg Allg Chem* 1954;**276**:209–26.